LWT - Food Science and Technology 129 (2020) 109564

Contents lists available at ScienceDirect

LWT - Food Science and Technology

journal homepage: www.elsevier.com/locate/lwt

A functional dairy product rich in Menaquinone-7 and FeOOH nanoparticles

Donya Novin[a], Jordan van der Wel[b], Mostafa Seifan[a], Alireza Ebrahiminezhad[c], Younes Ghasemi[d], Aydin Berenjian[a,*]

[a] School of Engineering, Faculty of Science and Engineering, The University of Waikato, Hamilton, 3216, New Zealand
[b] The TATUA Co-operative Dairy Company Limited, 3434 State Highway 26, Tatuanui, 3374, New Zealand
[c] Department of Medical Nanotechnology, School of Advanced Medical Sciences and Technologies, Shiraz University of Medical Sciences, Shiraz, Iran
[d] Department of Pharmaceutical Biotechnology, School of Pharmacy and Pharmaceutical Sciences Research Centre, Shiraz University of Medical Sciences, Shiraz, Iran

ARTICLE INFO

Keywords:
Menaquinone-7 fermentation
Iron oxide hydroxide nanoparticles
Functional food
Bacillus subtilis natto

ABSTRACT

Menaquinone-7 (MK-7) has been identified as an essential nutrient in enhancing bone mineral density, bone health, and reducing the risk of osteoporosis. Although there have been worthy achievements in MK-7 fermentation process using *Bacillus subtilis natto*, the low yield of fermentation, costly downstream extraction and purification processes remain the main challenges. In this research, a new approach was taken to study the feasibility of the production of a functional fermented dairy-based product rich in MK-7 by the use of iron oxide hydroxide (FeOOH) nanoparticles (NPs) to increase the concentration of MK-7. In this regard, milk a rich source of calcium, a necessary nutrient for bone health was chosen as the fermentation medium for MK-7 biosynthesis using *B. subtilis natto*. Two different types of FeOOH NPs, namely naked and biocompatible xanthan gum (XG)-coated NPs, were synthesised (with 10 nm average particle size) and used to evaluate their effect on developing a fermented dairy-based product rich in MK-7 and iron. According to the results, in the presence of 3 mg/L of XG-coated and 12 mg/L of naked FeOOH NPs, the concentration of MK-7 significantly enhanced, and approximately 27% and 35% more MK-7 biosynthesis were observed respectively as compared with control samples with only 1.9 mg/L MK-7 production.

1. Introduction

Osteoporosis and low bone mineral density (BMD) due to inadequate dietary intake of calcium and menaquinone-7 (MK-7) are the core causes of bone fractures and subsequent mortality. MK-7 is a subtype of vitamin K2 consist of a series of vitamers called menaquinones. The subtypes are characterised by the number of isoprenoid residues in their aliphatic side chains attached at the 3-position (n = 4–13) (Yamaguchi, 2014). Fig. 1 illustrates the molecular structure of menaquinone-7.

Natto (fermented soybean) is the richest source of MK-7 that could provide sufficient amount of MK-7 if it would get consumed in large quantities. It contains 796–939 μg/100g MK-7 which is superior to other known sources such as processed cheese and margarine with 0.3 and 0.1 μg/100g MK-7 respectively (Kamao et al., 2007). MK-7 is mainly synthesised through a fermentation process using *Bacillus subtilis* species with some process obstacles such as low yield and complicated costly recovery steps. Therefore, the development of functional food products with fewer recovery phases and boosted MK-7 concentration should be considered. The use of an appropriate fermentation medium and nutrients would be the key factor in enhancing the concentration of the intended functional ingredients. For this purpose, milk, a rich source of calcium (the building blocks of bones) has been used as the medium for *B.subtilis natto* fermentation to provide positive effects on consumers' health beyond the basic nutritional profile of milk.

On the other hand, studying the effect of iron NPs on enhancing MK-7 biosynthesis has become a new area of research to address the current challenges in MK-7 fermentation (Ebrahiminezhad, Varma, Yang, & Berenjian, 2016; Ebrahiminezhad, Varma, Yang, Ghasemi, & Berenjian, 2015). Iron is involved in numerous essential processes inside the bacterial cell, ranging from respiration, as both signalling molecules and enzymatic cofactors, to ribonucleotide synthesis due to the electronic structure of the iron atom, which can undergo reversible changes in its oxidation state (Guerinot, 1994). *B. subtilis* utilise three types of hydroxamate siderophores, including ferrichromes, ferrioxamines, and shizokinen, each taken up by different transport systems (Schneider & Hantke, 1993). Despite the abundance of iron in nature, iron often acts as a growth-limiting nutrient due to the low solubility of ferric iron under aerobic conditions at neutral pH (Bsat, Herbig, Casillas-Martinez, Setlow, & Helmann, 1998). *B. subtilis* modulates transcription in

* Corresponding author. School of Engineering, Faculty of Science and Engineering, The University of Waikato, Hamilton, New Zealand.
E-mail address: aydin.berenjian@waikato.ac.nz (A. Berenjian).

https://doi.org/10.1016/j.lwt.2020.109564
Received 6 March 2020; Received in revised form 6 May 2020; Accepted 6 May 2020
Available online 13 May 2020
0023-6438/ © 2020 Elsevier Ltd. All rights reserved.

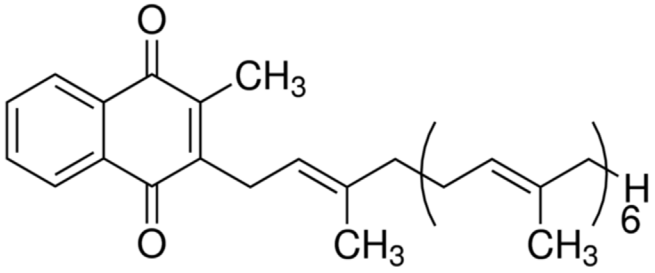

Fig. 1. Molecular structure of menaquinone-7.

response to changes in iron availability using the ferric uptake regulator (Fur) to sense intracellular iron availability and to maintain iron homeostasis (Pi & Helmann, 2017). According to a recent report, the presence of iron oxide NPs in the fermentation media has led to a 15% enhancement in MK-7 yield (Ebrahiminezhad et al., 2016).

The NPs are defined as particles with sizes ranging from 1 to 100 nm with unique properties that could not be found in bulk samples of the same material (Auffan et al., 2009). These metal NPs such as magnetite (Fe_3O_4), maghemite (γ-Fe_2O_3), hematite (α-Fe_2O_3), and goethite (FeOOH) can have properties such as high surface area, large surface-to-volume ratio, and easy separation under external magnetic fields (Cao et al., 2012; Xu et al., 2014). They are widely studied due to their unique applications in enzyme and protein immobilisation, magnetic resonance imaging (MRI), RNA and DNA purification, magnetic cell separation and purification, magnetically controlled transport of anti-cancer drugs, hyperthermia generation, process modification and intensification as well as in the food industry (Bazylinski, 1996; Durán & Marcato, 2013; Ebrahiminezhad et al., 2015, 2016; Kinoshita, Seino, Mizukoshi, Nakagawa, & Yamamoto, 2007; Laurent, Dutz, Häfeli, & Mahmoudi, 2011; Lee & Hyeon, 2012; Matsunaga, Sato, Kamiya, Tanaka, & Takeyama, 1999; Mornet et al., 2000; Pan, Gao, & Gu, 2005; Reetz, Zonta, Vijayakrishnan, & Schimossek, 1998; Taylor, Hurst, Davies, Sachsinger, & Bruce, 2000; Yu et al., 2008). However, apart from all the advantages, the uncoated form of NPs do not have sufficient physicochemical stability (poor solubility and biocompatibility) and are toxic to biological systems and environments (Kumar et al., 2014). Therefore, their surfaces need to be properly engineered to acquire improved biocompatibility and significantly eliminate their detrimental properties. The biocompatible coated NPs are among the Food and Drug Administration (FDA) approved nanostructures for biomedical applications (Anselmo & Mitragotri, 2016; Castaneda, Khurana, Khan, & Daldrup-Link, 2011) via introducing hydrophilic groups and modification of the bioinorganic shell on the surface of the NPs. The functional groups of coating materials introduced to iron NPs may also change their surface charge accordingly, which will affect the biological behaviours of NPs (Feng et al., 2018). This method can effectively optimise the properties of synthesised NPs to meet the requirements of the biomedical application. Among all mentioned iron NPs, FeOOH is one of the important iron NPs widely used for the treatment of Iron Deficiency Anaemia (IDA). Anaemia is defined by the World Health Organization (WHO) (2011) as a condition of insufficient red blood cells to meet physiological needs. It is a public health problem that needs to be addressed urgently since about 2.3 billion individuals are affected and nearly 1 billion suffer from IDA (Vos et al., 2016). There are four formulations of intravenous iron available in which all have an iron oxyhydroxide core and a carbohydrate coat (Verraes & Prenen, 2015). Iron NPs with neutral and hydrophilic carbohydrate shells with no toxicity are used instead of ferrous salts which frequently causes gastrointestinal side effects. However, the iron uptake through NPs with a negatively charged shell is nearly 40 times higher compared to NPs with neutral hydrophilic carbohydrate shell or ferric chloride and ferrous sulphate (Jahn et al., 2012).

Polysaccharides have the advantages of stability, water solubility and fewer side effects on the organism to be used as the modification and coating materials (Wang et al., 2018). Microbial polysaccharides such as bacterial cellulose (BC), dextrans, and xanthan gum (XG) have been widely used in the chemical, food, and pharmaceutical industries (Huang & Tang, 2007). Among them, XG has gained the leading microbial polysaccharide market due to its rheological features, as well as stability in a wide range of temperatures and pH (Huang & Tang, 2007). XG is an anionic, high molecular weight, exopolysaccharide (Pooja, Panyaram, Kulhari, Rachamalla, & Sistla, 2014). It is a microbial biopolymer produced by gram-negative bacteria of the genus *Xanthomonas* mainly by *Xanthomonas campestris* (Petri, 2015). It has been widely used in oral/topical formulations and drug release, cosmetics, cleaners, paints, and ceramic glazes. The most common use of XG is in the food industry as emulsifier, film-forming agent, stabilizing agent, and thickening agent in salad dressing, convenience and frozen foods, bakery products, as well as in dairy products (Alhalmi, Alzubaidi, Altowairi, Salem, & Sharma, 2017; Kar, Mohapatra, Bhanja, Das, & Barik, 2010; Kulkarni Vishakha, Butte Kishor, & Rathod Sudha, 2012; Petri, 2015). In addition, it is non-digestible in humans and provides lower calorific content of foods and improve their passage through the gastrointestinal tract (Katzbauer & Stability, 1998).

With respect to the benefits of iron NPs, this research aims to (i) synthesise a biocompatible iron NPs using a natural hetero-polysaccharide XG free from toxicity for human consumption; and (ii) investigate the effect of iron NPs on MK-7 biosynthesis and *B. subtilis natto* growth to demonstrate the possibility of developing a functional fermented milk rich in both MK-7 and iron.

2. Materials and methods

2.1. Chemicals

The ultra-high temperature (UHT) processed milk was purchased from the local market. 2-propanol and n-hexane, iron (III) chloride hexahydrate ($FeCl_3{\cdot}6H_2O$), and xanthan gum (XG) from *xanthomonas campestris* were purchased from Sigma-Aldrich Co., USA. Pure MK-7 was obtained from ChromaDex Co., USA for high-performance liquid chromatography (HPLC) analysis. Methanol was purchased from Scharlab S.L. Co., Spain. Lipopan F Conc BG enzyme was obtained from Novozymes (Novozymes Co., Denmark) and sodium chloride from a domestic supplier. Nutrient agar plates were purchased from Fort Richard Laboratories, Auckland, New Zealand.

2.2. Microorganism and inoculum preparation

The commercially available natto in the New Zealand market was used to isolate the *B. subtilis natto* strain. The bacterial cells were cultivated on nutrient agar plates (for 48h) and then were scraped off from the plates. Then, they were suspended in a sterilised saline solution (NaCl 0.9% w/v) and were kept in a water bath at 80 °C for 30 min and centrifuged at 1835 $\times$g for 10 min to remove the cell debris (Berenjian et al., 2011). The spore suspension of $2 \pm 0.5 \times 10^7$ CFU/mL was obtained and was kept in a fridge for the future fermentation experiments to be used as a starter culture.

2.3. MK-7 fermentation experiment

The fermentation process was carried out aerobically in 100 mL Erlenmeyer shake flasks by adding 50 mL of milk as the fermentation media. The fermentation was conducted at 38 °C, 140 RPM, and 1% (v/v) inoculum volume for three days. The range of NPs concentrations for fermentation experiments was selected based on the recommended daily allowance for iron. According to the National Institute of Health (National Institutes of Health: Office of Dietary Supplements, 2018), recommended dietary allowance for iron in healthy adults (19-50 year-old) is sex- and age-dependent and varies from 8 mg to 18 mg per day.

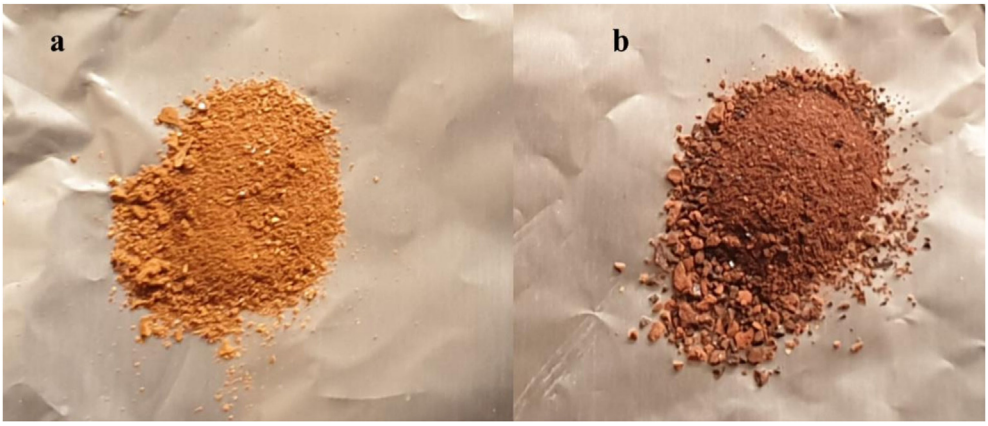

Fig. 2. Synthesised (a) naked NPs and (b) XG-coated iron oxide hydroxide NPs.

2.4. MK-7 extraction

The enzymatic treatment with a lipolytic enzyme (lipase) was carried out before extraction by adding 1% lipase powder to the 3 mL of sample and incubating at 37 °C. Then, the MK-7 was extracted from each sample using a mixture of n-hexane:2-propanol in the ratios of 2:1 (v/v) and 1:4 (liquid: organic (v/v)) (Berenjian et al., 2011). The mixture was vigorously shaken using a vortex mixer for 2 min and then centrifuged at 1835 ×g for 10 min to separate two phases. The upper hexane layer was separated and evaporate and the residues after evaporation were mixed with methanol for HPLC analysis.

2.5. High-performance liquid chromatography

The Thermo Scientific Dionex HPLC system equipped with a photodiode array UV detector (UVD 170U), AS1-100 automated sample injector, and four P680 pumps were used to measure the concentration of MK-7. A Phenomenex C18 Gemini column (5 μm, 150 × 4.6 mm, Phenomenex, USA) was used and operated at 40 °C and the flow rate of the mobile phase (methanol), the wavelength, and the injection volume were set at, 1 mL/min, 248 nm, and 60 μL respectively. The Chromeleon 7 software (Chromatography Data System) was used to control the system and for data acquisition.

2.6. Experimental design and statistical analysis

All the experimental values have been reported as mean value ± standard deviation (SD) of three replicates. Significant differences among the samples were determined using One-Way Analysis of Variance (One-Way ANOVA) followed by Tukey post hoc analysis. Statistical significance was accepted at $p < 0.05$.

2.7. Synthesis of naked and XG-coated iron oxide hydroxide nanoparticles

A chemical synthesis technique using iron salt ($FeCl_3{\cdot}6H_2O$) and 5M sodium hydroxide (NaOH) was used to fabricate FeOOH with homogenous composition and narrow size distribution. Briefly, 1.08 g of iron salt was added to 25 mL of deionised water in a round-bottomed flask. The flask with a magnetic stirrer in it was placed on a mixing plate at room temperature. Then, 30 mL of 5M NaOH was added to the mixture and gently mixed for 15 min, centrifuged at 815 ×g for 15 min, and then the supernatant was removed (Ghanbariasad et al., 2019). The precipitate was washed with deionised water (minimum 4 times) to remove the impurities. For the XG-coated NPs, the FeOOH was prepared by the hydrolysis of aqueous iron (III) chloride hexahydrate solution (FeCl3.6H2O) in the presence of XG at room temperature. Briefly, 0.25 g XG was dissolved in 25 mL deionised water and was gently stirred for 15 min. Afterwards, 1.08 g FeCl3.6H2O was added and to start the reaction, 30 mL 5M NaOH was rapidly injected under vigorous stirring, and the reaction was continued for 15 min. The produced nanoparticles were centrifuged at 1835 ×g for 20 min. After removing the supernatant, the precipitate was washed three times with deionised water to remove impurities. Both samples were dried in an oven at 50 °C overnight, ground into a powder form and kept in an airtight container for further use.

2.8. Characterisation of naked and coated iron nanoparticles

Characterisation of synthesised naked and coated iron nanoparticles was carried out using the following instruments. A transmission electron microscopy (TEM, Philips, CM10; HT 100 kV) was used to observe the morphology and size of the prepared NPs (Ebrahiminezhad et al., 2016; Seifan, Ebrahiminezhad, Ghasemi, Samani, & Berenjian, 2018a). Fourier transformed infrared spectroscopy (FTIR) (Bruker, Vertex 70, Kassel, Germany) using KBr pellets containing 1.5 mg sample and 15 mg KBr was used to characterise the fabricated nanoparticles. Measurements were done under ambient temperature in the exploration range of 4000 - 450 cm^{-1} (Seifan, Ebrahiminezhad, Ghasemi, Samani, & Berenjian, 2018b). Finally, X-ray diffraction (XRD) (Siemens D5000) with CuKα radiation at 45 kV and 40 mA was used to study the characteristics of synthesised nanoparticles. The well-dried NPs were backpacked into a sample holder and mounted onto the instrument sample changer. Data were collected at a step size of 0.0530° for a 2θ interval between 10° and 90° (Seifan, Samani, & Berenjian, 2017).

3. Results and discussion

3.1. Synthesis of naked and XG-coated iron NPs (FeOOH)

Naked FeOOH NPs were synthesised by the chemical precipitation method and subsequently coated with XG. Equation [1] explains the formation of FeOOH nanoparticles:

$$Fe^{+3} + 3OH^{-} \rightarrow Fe(OH)_3 \rightarrow FeOOH + H_2O \quad [1]$$

In this method, upon the addition of sodium hydroxide (NaOH) (as a precipitating agent) to the $FeCl_3.6H_2O$, a sudden colour change to yellow-brown was observed (Fig. 2(a)) due to the formation of FeOOH cores colloidal suspension upon hydrolysis of ferric ions (Ghanbariasad et al., 2019).

3.2. Characterisation of naked and XG-coated iron NPs

The morphology, size distribution of NPs were determined using a TEM. Fig. 3 shows the TEM images of the fabricated naked and XG-coated iron NPs. The TEM analysis of NPs revealed the production of

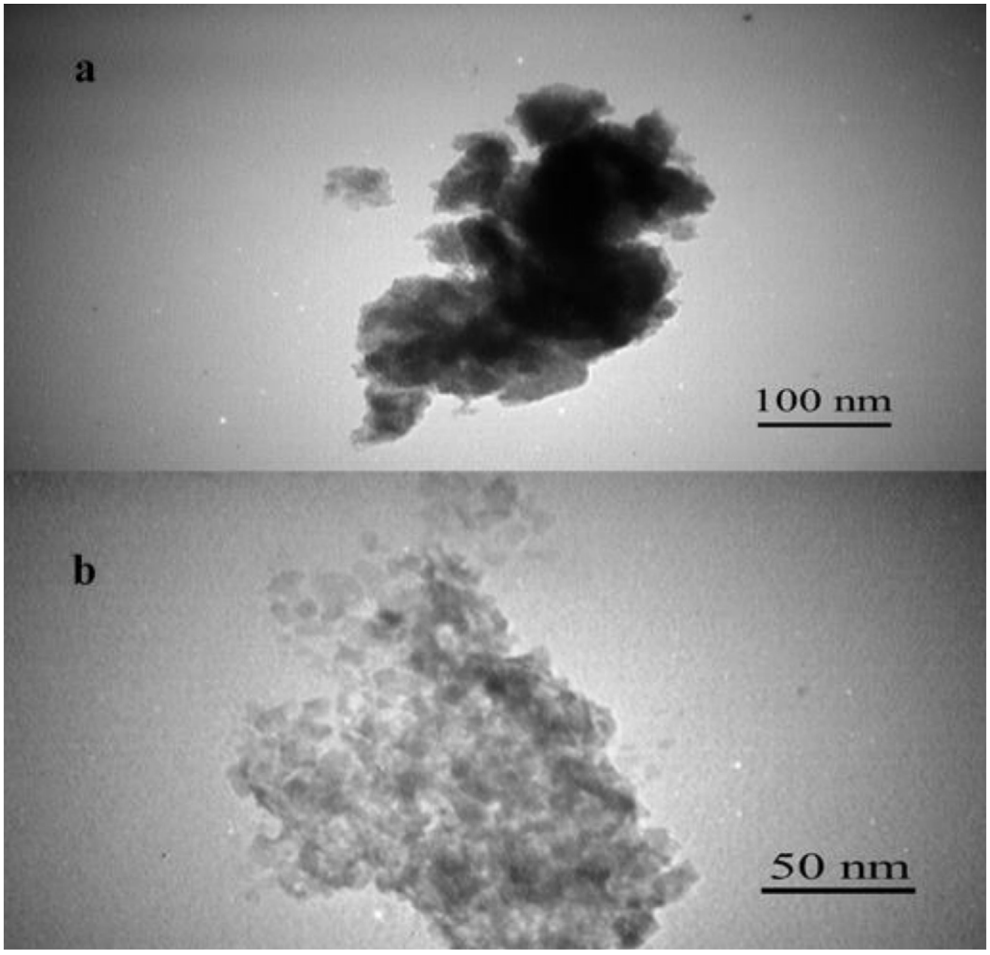

Fig. 3. Transmission electron micrograph (TEM) of the fabricated (a) naked and (b) XG-coated NPs.

uniform ultrafine NPs for both types of synthesised iron NPs. Particles size analyses were performed by means of ImageJ software version 1.47 v, an image analysis software (Ebrahiminezhad et al., 2017). The particles size distribution of both naked and XG-coated NPs was measured to be from 5 to 15 nm with 10 nm average particle size.

FTIR analysis was performed in order to figure out the functionality and the surface chemistry of the fabricated naked and XG-coated iron NPs. Fig. 4 (a) illustrates the FTIR spectra of the fabricated naked NPs. Fe–O characteristic peaks of NPs appeared at about 616 cm^{-1} (Ghanbariasad et al., 2019). The absorption at ~3362 cm^{-1} (stretching point) (Ghanbariasad et al., 2019) and 1339 cm^{-1} (deforming point) indicate the presence of O–H groups. The FTIR was also used to confirm the NPs coating functionalisation and the result is shown in Fig. 4 (b). The Fe–O characteristic peaks of NPs appeared at about 624 cm^{-1} (Ghanbariasad et al., 2019).

In the aqueous medium during precipitation synthesis, the surface of NPs are modified by O–H groups due to the coordination of unsaturated Fe atoms with water molecules and hydroxyl ions in both naked and XG-coated NPs (Ebrahiminezhad et al., 2012). The stretching vibrations of the O–H groups appeared at about 3419 cm^{-1}. In XG-coated NPs, the C–O stretching vibrations were seen at ~879 cm^{-1}. The peaks at 1434 and 1067 cm^{-1} showed the presence of carbonyl and C=C stretching vibration, respectively. The peak at 2500 cm^{-1} attributed to the aliphatic C–H groups. The obtained FTIR spectra exhibit a successful XG coating of iron NPs.

XRD was performed to characterise the fabricated naked and XG-coated NPs at 2θ between 10° and 90°. The XRD spectra of the prepared naked and coated NPs were validated by position and relative intensities of NPs (Fig. 5) at 2θ of about 34° and 64° as corresponded with the XRD diffraction peaks of standard FeOOH NPs.

3.3. Screening the effect of naked and XG-coated NPs on MK-7 production, bacterial growth, and pH

The impact of naked and XG-coated FeOOH NPs on MK-7 production was investigated by comparing the bacterial growth and pH changes in the absence and the presence of varying concentrations of naked and XG-coated iron NPs (3–12 mg/L). The NPs at different concentrations (3, 6, 9, and 12 mg/L) were mixed with milk and the fermentation was carried out. As depicted in Fig. 6 MK-7 production was affected by the presence of NPs in opposite ways for the samples containing naked and XG-coated NPs as compared to the control samples ($p < 0.05$). The increase in the concentration of naked NPs up to 12 mg/L resulted in the highest concentration of MK-7 (2.93 mg/L) while the lowest concentration of NPs (3 mg/L) resulted in a reduction (1.16 mg/L) in MK-7 biosynthesis as compared to control samples without nanoparticles (1.9 mg/L). In contrast, presence of XG-coated NPs at the lowest concentration (3 mg/L) led to the highest MK-7 production (2.63 mg/L) and a further increase in the concentration of XG-coated NPs to 12 mg/L resulted in lower MK-7 biosynthesis (1.85 mg/L).

As illustrated in Fig. 7, bacterial growth was also affected by the concentration of NPs. Increasing the naked NP concentrations from 3 mg/L to 12 mg/L resulted in a significant difference in cell growth ($p < 0.05$) compared to samples without any NPs. Bacterial growth was measured to be 14.2×10^7 CFU/mL when the fermentation media was supplemented with 12 mg/L naked NPs as compared to samples without NPs (10.4×10^7 CFU/mL). In comparison to the control

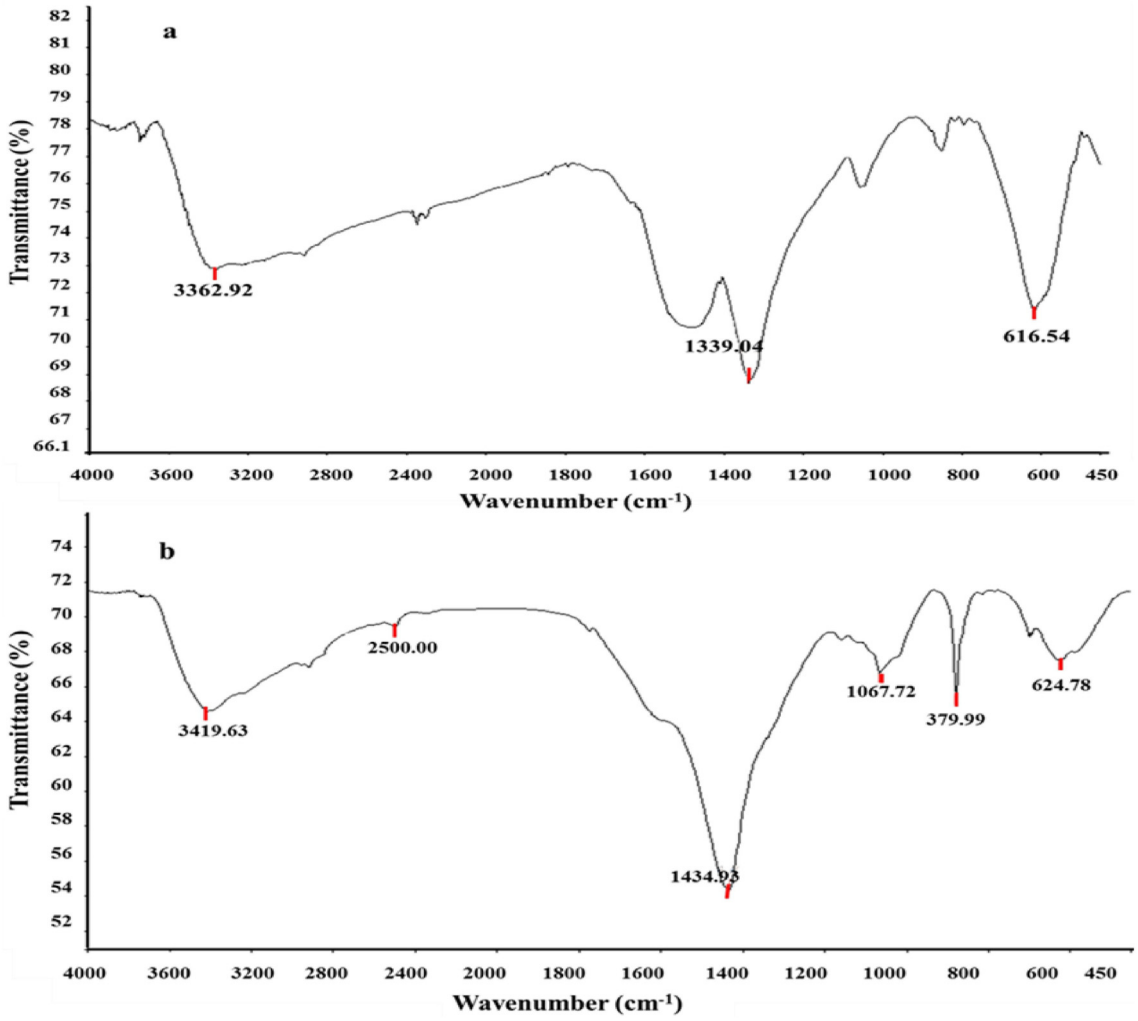

Fig. 4. FTIR of the (a) naked NPs (identified as Goethite crystals) and (b) XG-coated NPs.

samples, the lower concentrations of naked NPs (3, 6, and 9 mg/L) showed an inhibitory effect on bacterial growth by about 25%, 5%, and 13%, respectively. The highest bacterial growth was 15.2 × 10^7 CFU/mL (by adding 3 mg/L of XG-coated NPs) and a further increase in NP concentration lessened the cell growth by about 32%, 43%, and 32%, respectively as compared to control samples (10.4 × 10^7 CFU/mL). The results for both types of NPs showed that MK-7 production was bacterial growth dependant in which the more bacterial growth resulted in more MK-7 biosynthesis using *B. subtilis natto*.

Iron carries out several functions in the cell, mainly serving as signalling molecules and enzymatic cofactors (Guerinot, 1994). Generally, under physiological conditions, iron is found in one of two readily interconvertible redox states: the reduced Fe^{2+} ferrous form and the oxidised Fe^{3+} ferric form. In *B. subtilis,* the Fur protein is in charge of coordinating the expression of iron uptake and homeostasis pathways in response to available iron (Andrews, Robinson, & Rodríguez-Quiñones, 2003). Iron is an essential nutrient; however, it can be a growth-limiting nutrient due to the low solubility of ferric iron under aerobic conditions at neutral pH (Bsat, Herbig, Casillas-Martinez, Setlow, & Helmann, 1998Bsat, Herbig, Casillas-Martinez, Setlow, & Helmann, 1998). During this study, *B. subtilis* showed different behaviour in the presence of different concentrations of extracellular naked and XG-coated iron NPs. As there is not sufficient evidence to support the results, further studies at cell level are required to gain a better understanding of *B. subtilis natto* iron NP consumption.

The changes in pH over the course of fermentation is shown in Fig. 8. For all samples, there was an increase in pH to above 8 compared to control samples showing an increase from the initial pH of 6.5 to pH 7 at the end of fermentation.

3.4. Monitoring the MK-7 biosynthesis, bacterial growth, and pH in the presence of XG-coated iron NPs over the course of fermentation

According to the results of screening, the concentration of 3 mg/L coated and 12 mg/L naked iron NPs showed the highest MK-7 production and bacterial growth in comparison with control samples without NPs. Considering the toxicity of naked iron NPs and the advantage of the iron-polysaccharide complex including good tolerability, bioavailability, and higher percentage content of iron (Zhang & Liu, 2011), the samples containing XG-coated NPs (3 mg/L) were monitored. The MK-7 biosynthesis, bacterial growth, and pH changes were monitored throughout fermentation for three days. According to Fig. 9 and Fig. 10, MK-7 production was growth-dependent and as the growth phase entered the exponential phase, the MK-7 concentration started to increase. During the exponential growth phase, MK-7 increased at a steady pace and increased by about 30%. The MK-7 concentration increased from 1.61 mg/L at the beginning of the exponential growth phase to 2.47 mg/L by the end of that phase.

The changes in pH during the three days of fermentation are illustrated in Fig. 11. The pH increased from 6.70 at the beginning of fermentation to 8.26 by the end of it. The pH change followed the same trend as all other experiments carried out in this research. The

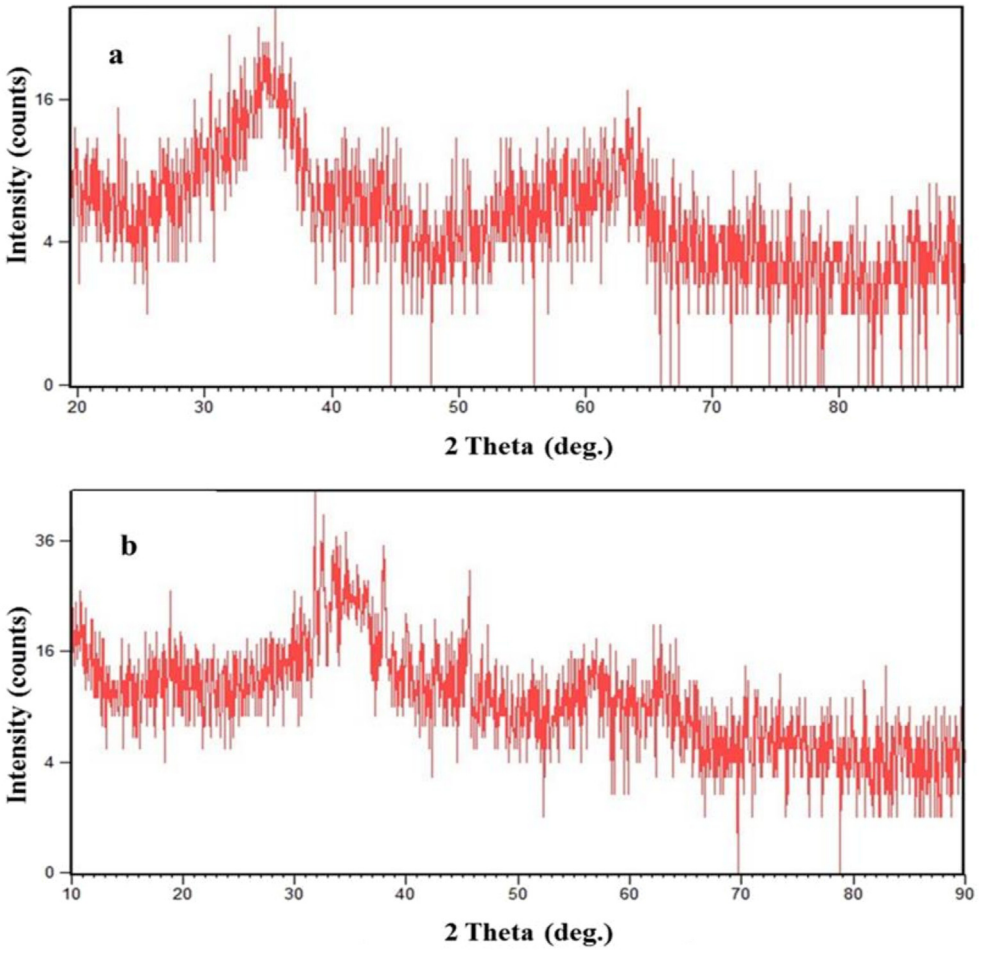

Fig. 5. X-ray diffraction (XRD) pattern of the synthesised (a) naked NPs and (b) coated NPs with XG.

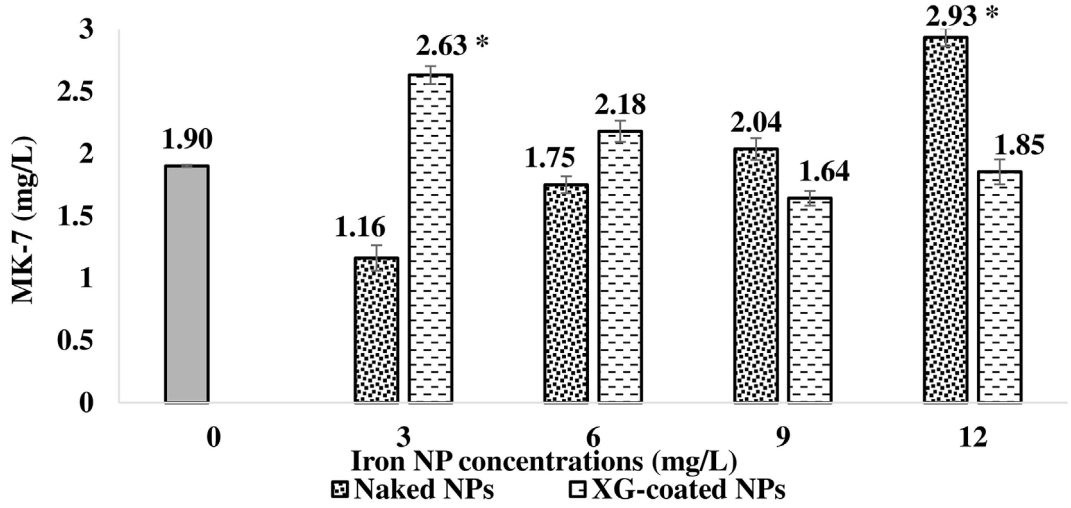

Fig. 6. MK-7 production at various concentrations (0–12 mg/L) of naked and XG-coated NPs. * denotes significance of difference at $p < 0.05$ compared with the control.

enhancement in MK-7 production was related to an increase in pH, up to about pH 8 due to proteolysis of the proteins by *B. subtilis*.

3.5. Future studies

This research provides novel information on MK-7 production and the application of nanotechnology, in particular, food-grade nanoparticles in food processing. This advancement in the presence of biocompatible iron NPs could be used to develop a variety of fermented functional foods rich in MK-7 and iron NPs and to enhance further all aspects of food processing from improved health benefits to improved taste and texture.

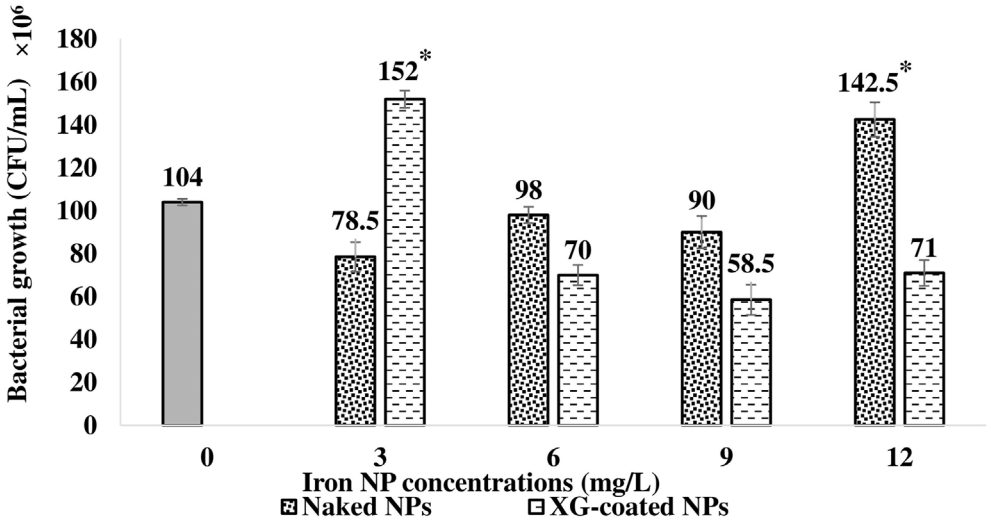

Fig. 7. Bacterial growth at various concentrations (0–12 mg/L) of naked and XG-coated NPs. * denotes significance of difference at $p < 0.05$ compared with the control.

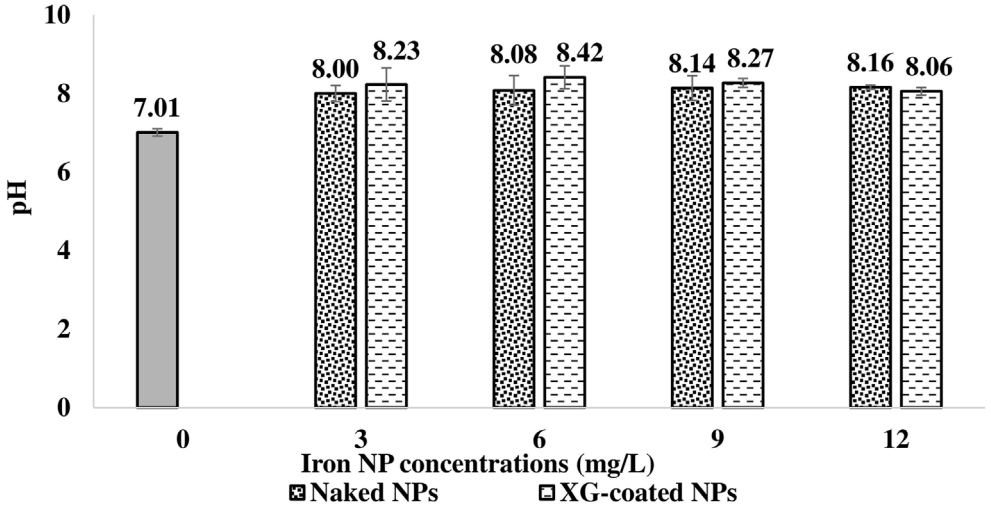

Fig. 8. pH change at various concentrations of naked and XG-coated NPs (0–12 mg/L).

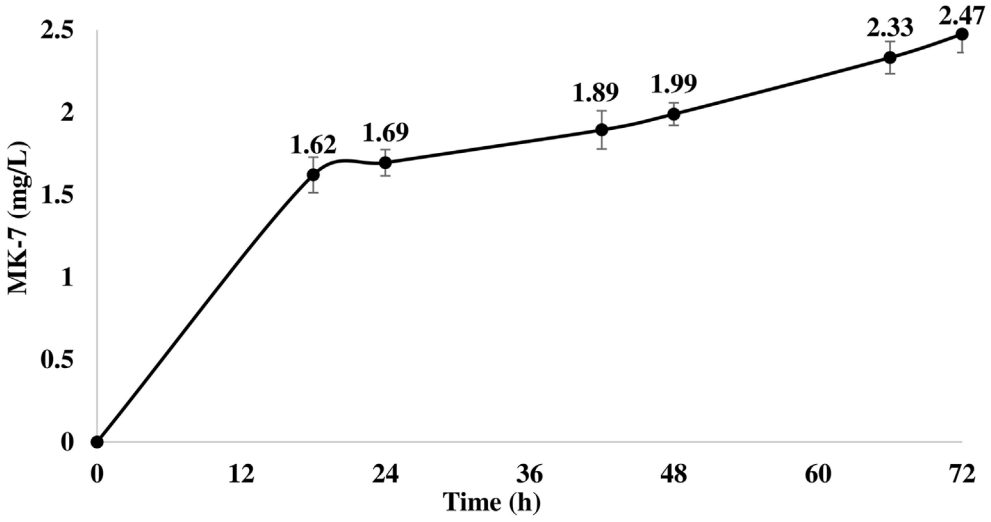

Fig. 9. Changes in MK-7 concentration during the time course of fermentation at 3 mg/L of XG-coated NPs.

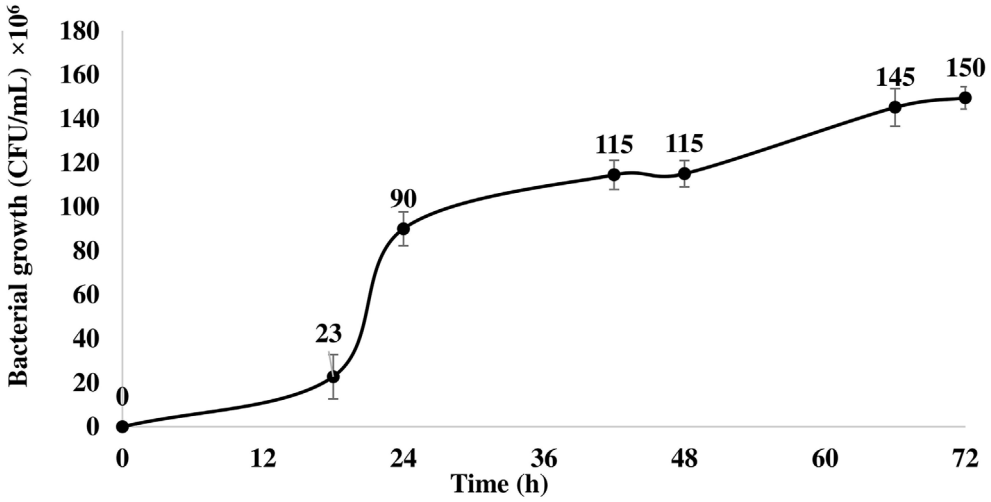

Fig. 10. Changes in bacterial growth during the time course of fermentation at 3 mg/L of XG-coated NPs.

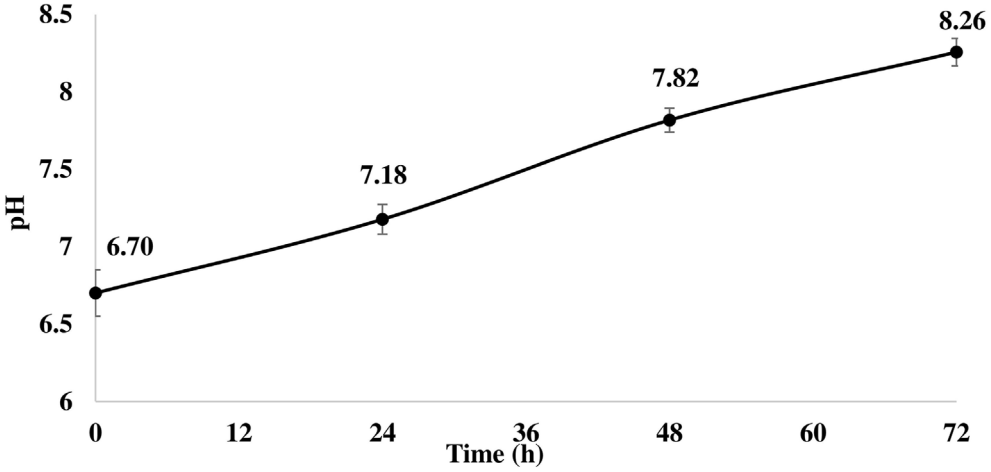

Fig. 11. Changes in pH during the course of fermentation at 3 mg/L of XG-coated NPs.

4. Conclusion

The naked and XG-coated iron NPs were successfully synthesised and characterised. The results confirmed that the fabricated NPs were uniform and monodisperse, and the XG coating had no negative effect on the size of fabricated NPs. The fermentation process was performed to investigate the effect of iron oxide hydroxide NPs on *B. subtilis* growth, MK-7 production, and pH changes. It was shown that the addition of naked and XG-coated NPs at highest and lowest concentrations (12 mg/L and 3 mg/L) respectively could significantly increase the MK-7 production by improving bacterial growth. Based on the results, XG-coated NPs are recommended to be used as the MK-7 biosynthesis booster for the production of a novel fermented dairy-based product rich in MK-7 and iron NPs.

CRediT authorship contribution statement

Donya Novin: Data curation, Writing - original draft, Conceptualization, Methodology, Software. **Jordan van der Wel:** Supervision, Writing - review & editing, Resources. **Mostafa Seifan:** Supervision, Writing - review & editing. **Alireza Ebrahiminezhad:** Visualization, Investigation. **Younes Ghasemi:** Methodology. **Aydin Berenjian:** Supervision, Methodology, Writing - review & editing, Resources.

Declaration of competing for interest

The authors declare that there is no conflict of interest associated with this publication.

Acknowledgements

This work was financially supported by Callaghan Innovation and Tatua Co-Operative Dairy Company Ltd, New Zealand.

References

Alhalmi, A., Alzubaidi, N., Altowairi, M., Salem, M., & Sharma, B. (2017). Xanthan gum; its biopharmaceutical applications: An overview. *World Journal of Pharmacy and Pharmaceutical Sciences, 7*, 1536–1548.

Andrews, S. C., Robinson, A. K., & Rodríguez-Quiñones, F. (2003). Bacterial iron homeostasis. *FEMS Microbiology Reviews, 27*, 215–237.

Anselmo, A. C., & Mitragotri, S. (2016). Nanoparticles in the clinic. *Bioengineering & Translational Medicine, 1*, 10–29.

Auffan, M., Rose, J., Bottero, J.-Y., Lowry, G. V., Jolivet, J.-P., & Wiesner, M. R. (2009). Towards a definition of inorganic nanoparticles from an environmental, health and safety perspective. *Nature Nanotechnology, 4*, 634.

Bazylinski, D. A. (1996). Controlled biomineralization of magnetic minerals by magnetotactic bacteria. *Chemical Geology, 132*, 191–198.

Berenjian, A., Mahanama, R., Talbot, A., Biffin, R., Regtop, H., Valtchev, P., et al. (2011). Efficient media for high menaquinone-7 production: Response surface methodology approach. *New Biotech, 28*, 665–672.

Bsat, N., Herbig, A., Casillas-Martinez, L., Setlow, P., & Helmann, J. D. (1998). Bacillus subtilis contains multiple Fur homologues: Identification of the iron uptake (Fur) and

peroxide regulon (PerR) repressors. *Molecular Microbiology, 29*, 189–198.
Cao, M., Li, Z., Wang, J., Ge, W., Yue, T., Li, R., et al. (2012). Food related applications of magnetic iron oxide nanoparticles: Enzyme immobilization, protein purification, and food analysis. *Trends in Food Science & Technology, 27*, 47–56.
Castaneda, R. T., Khurana, A., Khan, R., & Daldrup-Link, H. E. (2011). Labeling stem cells with ferumoxytol, an FDA-approved iron oxide nanoparticle. *Journal of Visualized Experiments*e3482.
Durán, N., & Marcato, P. D. (2013). Nanobiotechnology perspectives. Role of nanotechnology in the food industry: A review. *International Journal of Food Science and Technology, 48*, 1127–1134.
Ebrahiminezhad, A., Davaran, S., Rasoul-Amini, S., Barar, J., Moghadam, M., & Ghasemi, Y. (2012). Synthesis, characterization and anti-listeria monocytogenes effect of amino acid coated magnetite nanoparticles. *Current Nanoscience, 8*, 868–874.
Ebrahiminezhad, A., Varma, V., Yang, S., & Berenjian, A. (2016). Magnetic immobilization of Bacillus subtilis natto cells for menaquinone-7 fermentation. *Applied Microbiology and Biotechnology, 100*, 173–180.
Ebrahiminezhad, A., Varma, V., Yang, S., Ghasemi, Y., & Berenjian, A. (2015). Synthesis and application of amine functionalized iron oxide nanoparticles on menaquinone-7 fermentation: A step towards process intensification. *Nanomaterials (Basel, Switzerland), 6*, 1.
Ebrahiminezhad, A., Zare, M., Kiyanpour, S., Berenjian, A., Niknezhad, S. V., & Ghasemi, Y. (2017). Biosynthesis of xanthan gum-coated INPs by using Xanthomonas campestris. *IET Nanobiotechnology, 12*, 254–258.
Feng, Q., Liu, Y., Huang, J., Chen, K., Huang, J., & Xiao, K. (2018). Uptake, distribution, clearance, and toxicity of iron oxide nanoparticles with different sizes and coatings. *Scientific Reports, 8*, 2082.
Ghanbariasad, A., Taghizadeh, S.-M., Show, P. L., Nomanbhay, S., Berenjian, A., Ghasemi, Y., et al. (2019). Controlled synthesis of iron oxyhydroxide (FeOOH) nanoparticles using secretory compounds from Chlorella vulgaris microalgae. *Bioengineered, 10*, 390–396.
Guerinot, M. L. (1994). Microbial iron transport. *Annual Review of Microbiology, 48*, 743–772.
Huang, W.-C., & Tang, I.-C. (2007). Bacterial and yeast cultures–process characteristics, products, and applications. *Bioprocessing for value-added products from renewable Resources* (pp. 185–223). Elsevier.
Jahn, M. R., Nawroth, T., Fütterer, S.r., Wolfrum, U., Kolb, U., & Langguth, P. (2012). Iron oxide/hydroxide nanoparticles with negatively charged shells show increased uptake in Caco-2 cells. *Molecular Pharmaceutics, 9*, 1628–1637.
Kamao, M., Suhara, Y., Tsugawa, N., Uwano, M., Yamaguchi, N., Uenishi, K., et al. (2007). Vitamin K content of foods and dietary vitamin K intake in Japanese young women. *Journal of Nutritional Science and Vitaminology, 53*, 464–470.
Kar, R., Mohapatra, S., Bhanja, S., Das, D., & Barik, B. (2010). Formulation and in vitro characterization of xanthan gum-based sustained release matrix tables of isosorbide-5-mononitrate. *Iranian Journal of Pharmaceutical Research: IJPR, 9*, 13.
Katzbauer, B. J. P.d., & Stability (1998). Properties and applications of xanthan gum. *Polymer Degradation and Stability, 59*, 81–84.
Kinoshita, T., Seino, S., Mizukoshi, Y., Nakagawa, T., & Yamamoto, T. A. (2007). Functionalization of magnetic gold/iron-oxide composite nanoparticles with oligonucleotides and magnetic separation of specific target. *Journal of Magnetism and Magnetic Materials, 311*, 255–258.
Kulkarni Vishakha, S., Butte Kishor, D., & Rathod Sudha, S. (2012). Natural polymers–A comprehensive review. *International Journal of Research in Pharmaceutical and Biomedical Sciences, 3*, 1597–1613.
Kumar, N., Omoregie, E. O., Rose, J., Masion, A., Lloyd, J. R., Diels, L., et al. (2014). Inhibition of sulfate reducing bacteria in aquifer sediment by iron nanoparticles. *Water Research, 51*, 64–72.
Laurent, S., Dutz, S., Häfeli, U. O., & Mahmoudi, M. (2011). Magnetic fluid hyperthermia: Focus on superparamagnetic iron oxide nanoparticles. *Advances in Colloid and Interface Science, 166*, 8–23.
Lee, N., & Hyeon, T. (2012). Designed synthesis of uniformly sized iron oxide nanoparticles for efficient magnetic resonance imaging contrast agents. *Chemical Society Reviews, 41*, 2575–2589.
Matsunaga, T., Sato, R., Kamiya, S., Tanaka, T., & Takeyama, H. (1999). Chemiluminescence enzyme immunoassay using ProteinA-bacterial magnetite complex. *Journal of Magnetism and Magnetic Materials, 194*, 126–131.
Mornet, S., Vekris, A., Bonnet, J., Duguet, E., Grasset, F., Choy, J. H., et al. (2000). DNA–magnetite nanocomposite materials. *Materials Letters, 42*, 183–188.
National Institutes of Health: Office of Dietary Supplements. (2018). Iron: Fact sheet for health professionals. https://ods.od.nih.gov/factsheets/Iron-HealthProfessional.
Pan, B.-f., Gao, F., & Gu, H.-c. (2005). Dendrimer modified magnetite nanoparticles for protein immobilization. *Journal of Colloid and Interface Science, 284*, 1–6.
Petri, D. F. (2015). Xanthan gum: A versatile biopolymer for biomedical and technological applications. *Journal of Applied Polymer Science, 132*.
Pi, H., & Helmann, J. D. (2017). Sequential induction of Fur-regulated genes in response to iron limitation in Bacillus subtilis. *Proceedings of the National Academy of Sciences, 114*, 12785–12790.
Pooja, D., Panyaram, S., Kulhari, H., Rachamalla, S. S., & Sistla, R. (2014). Xanthan gum stabilized gold nanoparticles: Characterization, biocompatibility, stability and cytotoxicity. *Carbohydrate Polymers, 110*, 1–9.
Reetz, M. T., Zonta, A., Vijayakrishnan, V., & Schimossek, K. (1998). Entrapment of lipases in hydrophobic magnetite-containing sol-gel materials: Magnetic separation of heterogeneous biocatalysts1Dedicated to prof. Herman van Bekkum on the occasion of his 65th birthday.1. *Journal of Molecular Catalysis A: Chemical, 134*, 251–258.
Schneider, R., & Hantke, K. (1993). Iron-hydroxamate uptake systems in Bacillus subtilis: Identification of a lipoprotein as part of a binding protein-dependent transport system. *Molecular Microbiology, 8*, 111–121.
Seifan, M., Ebrahiminezhad, A., Ghasemi, Y., Samani, A. K., & Berenjian, A. (2018a). Amine-modified magnetic iron oxide nanoparticle as a promising carrier for application in bio self-healing concrete. *Applied Microbiology and Biotechnology, 102*, 175–184.
Seifan, M., Ebrahiminezhad, A., Ghasemi, Y., Samani, A. K., & Berenjian, A. (2018b). The role of magnetic iron oxide nanoparticles in the bacterially induced calcium carbonate precipitation. *Applied Microbiology and Biotechnology, 102*, 3595–3606.
Seifan, M., Samani, A. K., & Berenjian, A. (2017). A novel approach to accelerate bacterially induced calcium carbonate precipitation using oxygen releasing compounds (ORCs). *Biocatalysis and Agricultural Biotechnology, 12*, 299–307.
Taylor, J. I., Hurst, C. D., Davies, M. J., Sachsinger, N., & Bruce, I. J. (2000). Application of magnetite and silica–magnetite composites to the isolation of genomic DNA. *Journal of Chromatography A, 890*, 159–166.
Verraes, K., & Prenen, H. (2015). Iron deficiency in gastrointestinal oncology. *Annals of Gastroenterology, 28*, 19–24.
Vos, T., Allen, C., Arora, M., Barber, R. M., Bhutta, Z. A., Brown, A., et al. (2016). Global, regional, and national incidence, prevalence, and years lived with disability for 310 diseases and injuries, 1990–2015: A systematic analysis for the global burden of disease study 2015. *The Lancet, 388*, 1545–1602.
Wang, K., Li, L., Xu, X., Lu, L., Wang, J., Wang, S., et al. (2018). Fe_3O_4@ astragalus polysaccharide core-shell nanoparticles for iron deficiency anemia therapy and magnetic resonance imaging in vivo. *ACS Applied Materials & Interfaces, 11*, 10452–10461.
World Health Organization (2011). Haemoglobin concentrations for the diagnosis of anaemia and assessment of severity. https://apps.who.int/iris/handle/10665/85839, Accessed date: 29 August 2019.
Xu, J., Sun, J., Wang, Y., Sheng, J., Wang, F., & Sun, M. (2014). Application of iron magnetic nanoparticles in protein immobilization. *Molecules, 19*, 11465.
Yamaguchi, M. (2014). Role of nutritional factor menaquinone-7 in bone homeostasis and osteoporosis prevention. *Integr. Mol. Med. 1*, 1–6.
Yu, M. K., Jeong, Y. Y., Park, J., Park, S., Kim, J. W., Min, J. J., et al. (2008). Drug-loaded superparamagnetic iron oxide nanoparticles for combined cancer imaging and therapy in vivo. *Angewandte Chemie, 120*, 5442–5445.
Zhang, Y.-Y., & Liu, J.-h. (2011). Optimization of process conditions for preparing an iron-polysaccharide complex by response surface methodology. *Chemical and Biochemical Engineering Quarterly, 25*, 75–81.